



OPEN ACCESS

EDITED BY

Fajin Chen,
Guangdong Ocean University, China

REVIEWED BY

Xiaozhong Huang,
Lanzhou University, China
Liang Zhou,
Jiangsu Normal University, China

*CORRESPONDENCE

Zhongping Lai
zhongping_lai@stu.edu.cn
Xiaolin Xu
xiaolinxu_geo@163.com

SPECIALTY SECTION

This article was submitted to
Marine Biogeochemistry,
a section of the journal
Frontiers in Marine Science

RECEIVED 30 August 2022

ACCEPTED 20 October 2022

PUBLISHED 16 November 2022


CITATION

Lin P, Xu X, Yan C, Luo L, Abbas M
and Lai Z (2022) Holocene
sedimentary of the Pearl River Delta in
South China: OSL and radiocarbon
dating of cores from Zhuhai.
Front. Mar. Sci. 9:1031456.
doi: 10.3389/fmars.2022.1031456

COPYRIGHT

© 2022 Lin, Xu, Yan, Luo, Abbas and Lai.
This is an open-access article
distributed under the terms of the
[Creative Commons Attribution License
\(CC BY\)](https://creativecommons.org/licenses/by/4.0/). The use, distribution or
reproduction in other forums is
permitted, provided the original
author(s) and the copyright owner(s)
are credited and that the original
publication in this journal is cited, in
accordance with accepted academic
practice. No use, distribution or
reproduction is permitted which does
not comply with these terms.

Holocene sedimentary of the Pearl River Delta in South China: OSL and radiocarbon dating of cores from Zhuhai

Penghui Lin¹, Xiaolin Xu^{1*}, Chaoyang Yan², Lan Luo³,
Mahmoud Abbas ¹ and Zhongping Lai^{1,4*}

¹Institute of Marine Sciences, Guangdong Provincial Key Laboratory of Marine Disaster Prediction and Prevention, Shantou University, Shantou, China, ²School of Earth Sciences, China University of Geosciences, Wuhan, China, ³Department of Physics, Purdue Rare Isotope Measurement Laboratory, Purdue University, West Lafayette, IN, United States, ⁴Southern Marine Science and Engineering Guangdong Laboratory (Zhuhai), Zhuhai, China

Deltaic sediments provide a window for investigating delta development processes and the effects of human activities. Despite the fact that numerous studies have been conducted in the Pearl River Delta (PRD), the chronological data are still very limited, which hinder the detailed interpretation of the sedimentary records. The current study aims to establish high-resolution chronology on two cores from Zhuhai using quartz optically stimulated luminescence (OSL) and radiocarbon (¹⁴C) dating and, further, to reconstruct the Holocene sedimentary history of the PRD. Core P1-1 has a depth of 79 m and core P3-2 a depth of 60 m. Thirteen quartz OSL samples from P1-1 produced ages between 10.4 and 0.16 ka. Eight OSL and eight ¹⁴C ages from P3-2 span from 10.7 to 0.3 ka. The OSL and ¹⁴C dates show a good agreement above the depth of 26 m (1.4–0.3 ka), but with discrepancies at depths of 26–54 m. ¹⁴C ages (10.7–8.1 ka) are generally older (up to c. 2 ka) than quartz OSL ages, and the discrepancy decreases with depth. The age model shows three phases of the sedimentation process: (1) rapid accumulation rates of 7.48 (P1-1) and 7.52 (P3-2) m/ka between c. 10.7 and 7.5 ka in response to high sea level, (2) followed by a significantly reduced rate of 2.24 m/ka (P1-1) and a depositional hiatus (P3-2) from 7.5 to 2.5 ka as a result of reduced sediment supply and strong scouring by tidal processes, and (3) high sedimentation rates of 8.86 (P1-1) and 9.07 (P3-2) m/ka since 2.5 ka associated with intensive human activities and weakening tidal hydrodynamics. This sedimentary pattern is also evident in many other Asian deltas.

KEYWORDS

Pearl River Delta, optically stimulated luminescence dating, radiocarbon dating, sedimentation rate, global change

1 Introduction

Coastal deltas are important sedimentary records for understanding palaeo-environmental changes in land–sea interaction areas in response to sea level variations (Saito et al., 1998; McLean and Tsyban, 2001; Woodroffe et al., 2006; Bianchi and Allison, 2009). Rapid sea level rise is considered as the main driver worldwide for the formation of deltas during the early Holocene (Stanley and Warne, 1994). The rising seawater penetrated into the incised valleys that formed during the last glacial maximum (LGM) (Hori and Saito, 2007; Tamura et al., 2009) and created an accommodation space for deltaic development (Zong et al., 2012; Xu et al., 2019; Wang et al., 2022). Subsequently, as the sea level forcing was almost eliminated by 7 cal ka BP, fluvial runoff and tidal currents controlled the delta progradation (Woodroffe, 2000; Saito et al., 2001; Hori et al., 2002; Zong et al., 2009a).

The Pearl River Delta (PRD) is one of the largest coastal deltas in the world. Boreholes and high-resolution seismic profiles demonstrated that a major marine sequence was deposited in the PRD during the Holocene (Fyfe et al., 1997; Owen et al., 1998; Zong et al., 2009a; Xu et al., 2020). Over the past two decades, several studies have attempted to reconstruct the Holocene evolutionary history of the PRD and elucidated the driving mechanisms by investigating the Holocene strata at different time scales and regional settings (Zong et al., 2009a; Zong et al., 2012; Wu et al., 2017; Xiong et al., 2018a; Fu et al., 2020; Xiong et al., 2020; Xu et al., 2020). For instance six stratigraphic transects from the head area through the central basin to northern estuaries were used to investigate the interactions between sea level rise, monsoon runoff, and the palaeo-landscape in the early Holocene (Zong et al., 2012). Middle Holocene studies have focused on the factors that led to low sedimentation rates and slow progradation in central deltaic plain (Zong et al., 2009a; Fu et al., 2020). For the late Holocene, Xiong et al. (2020) found a rise in land growth rate from 0.36–0.38 to 2.69–10.56 km²/a, *i.e.*, accelerated coastline advances after c. 2.2 ka using historical archives, genealogical books, and modern survey data. It has been hypothesized to be triggered by agricultural activities and land reclamation with strong human influence, as shown by organic and inorganic geochemical indicators (Zong et al., 2010; Hu et al., 2013) and bathymetric data (Wu et al., 2016).

Despite the fact that a relatively clear understanding of Holocene landform development has been established based on numerous records mentioned above, studies on the sedimentation processes of the southern estuary are limited. The Modaomen estuary, for example, is the largest mouth of the Pearl River (Huang et al., 1982; He et al., 2022), but relevant sedimentation research is scarce (Zong et al., 2009b; Lu et al., 2020). Earlier research suggested that sedimentary records from estuary sites could provide information about the palaeo-environment evolution in response to natural and human

impacts during the Holocene (Wu et al., 2017; Xiong et al., 2018b; Chen et al., 2019). Therefore, a better knowledge of the deltaic–estuarine sedimentation process is of great importance and may shed light on the interpretation of the evolutionary history of the PRD.

An accurate chronology of delta sediments is pivotal to understanding palaeo-environmental changes. The published ages of the PRD sediments have mainly been based on radiocarbon dating (Huang et al., 1982; Li et al., 1991; Zong et al., 2006; Hu et al., 2013; Wu et al., 2017). However, the carbon reservoir effect of the carbonate-rich PRD region can yield abnormal ¹⁴C ages by releasing negative particulate organic carbon to depositional process (Liu et al., 2017). For instance the ¹⁴C ages are generally older than OSL ages at similar depths in core DA from the southern PRD, and this discrepancy might be caused by the carbon reservoir effect (Xu et al., 2020). In addition, reworking of carbon materials in deltas with complex hydrodynamics usually causes overestimation of radiocarbon ages, which can be abnormally old by up to 2 ka for surface samples (Yim et al., 2006; Kong et al., 2014). Recently, optically stimulated luminescence (OSL) dating has been recognized as an invaluable method for dating coastal sediments (Yi et al., 2012; Wang et al., 2013; Yi et al., 2014; Gao et al., 2016; Wang et al., 2018; Wang et al., 2019; Xu et al., 2020; Nian et al., 2021; Xu et al., 2022; Long et al., 2022; Wang et al., 2022). In addition, multi-dating technique, such as OSL and ¹⁴C dating, has been applied in Holocene deltaic sediments, *e.g.*, from the Yangtze River delta (Nian et al., 2021) and the PRD (Xu et al., 2020), and found to be appropriate for establishing comprehensive chronostratigraphic sequences.

In this study, cores P1-1 and P3-2, drilled from the estuary of the southern PRD, were dated by OSL and accelerator mass spectrometry (AMS) ¹⁴C techniques to build a high-resolution chronological framework. Together with the analyses of sedimentological characteristics and sedimentation rates, the Holocene sedimentary history of the PRD was reconstructed.

2 Study area and samples

2.1 Study area

The Pearl River delta is located in the south-central part of Guangdong Province and faces the South China Sea (Figure 1A). The palaeo-Pearl River had evolved to a configuration similar to the present in the early Miocene (He et al., 2020). During the late Quaternary, active faulting and differential uplifting processes resulted in an expansion of accommodation for receiving sediments from drainage basins and marine transgressions (Huang et al., 1982; Yu et al., 2016). Since the Holocene, the fault activity in the PRD became weaker, and the river system basically inherited the pattern before the last marine transgression (Yao et al., 2013). Limited by the altitude of

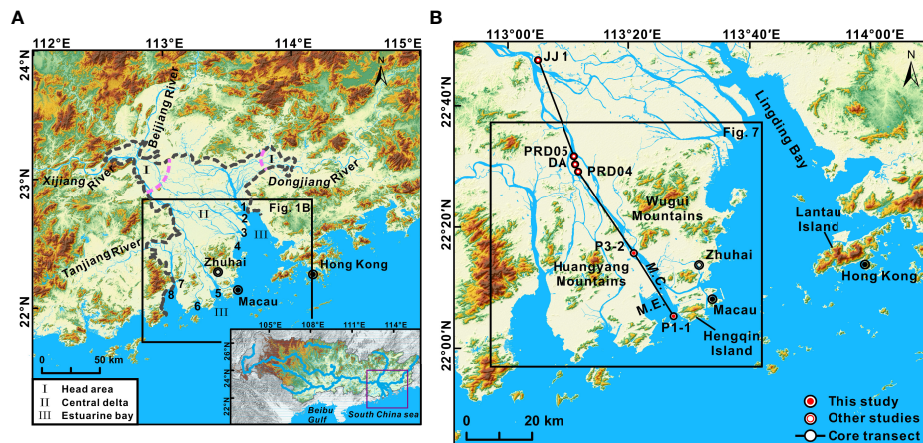


FIGURE 1

(A) Topographic characteristics of the Pearl River Delta (PRD). The PRD is divided into head area (zone I), central basin (zone II), and estuarine bay (zone III). Numbers 1–8 represent the eight estuaries of the PRD, namely, Humen, Jiaomen, Hongqimen, Hengmen, Modaomen, Jitimen, Hutiaomen, and Yamen, respectively. The inset figure shows the drainage system of the Pear River. (B) Topographic characteristics of the southern PRD, together with the locations of cores P1-1 and P3-2 (this study) and others reported: core JJ1 (Zong et al., 2009a), core PRD05 (Liu et al., 2008), core DA (Xu et al., 2020), and core PRD04 (Wei and Wu, 2011). M.E. and M.C. indicate the Modaomen Estuary and Modaomen Channel, respectively.

basement bedrock, the thickness of Quaternary sediments in the PRD varies between 10 to 40 m on average and reaches up to 60 m in incised valleys from Xijiang River and Beijiang River deltas (Huang et al., 1982).

The PRD can be divided into the head area, central delta, and estuarine bay according to the distance toward the sea (Figure 1A; Zong et al., 2009a). The water and sediments enter the dense distributary networks and flow out into the ocean through eight main outlets of the PRD (Wei and Wu, 2011). The outlets are morphologically separated by Wugui Mountains into two parts, *i.e.*, Humen, Jiaomen, Hongqimen, and Hengmen in the east and Modaomen, Jitimen, Hutiaomen, and Yamen in the west (Figure 1A). Among these outlets, the Modaomen estuary features the highest flood discharge and sand transport rates (He et al., 2022). The vast palaeo-Modaomen estuary contained a series of bi-directional jet systems which played an important role to the formation of sandbars and the major seaward channel of Xijiang River (Wu et al., 2007). The modern Modaomen estuary is under a stage of weakened estuarine jet (Wu et al., 2010). Due to the artificial deposition-promoting activities and land reclamations, the coastlines of the Modaomen estuary expanded seaward at a rate of 24 m/a during 1976–2006 AD (Zhang et al., 2015).

2.2 Sediment cores and sampling

Cores P1-1 [22°5′34.08″ N, 113°27′24.48″ E, 6 m below the present sea level (bpsl)] and P3-2 (22°15′42.99″ N, 113°20′59.87″ E, 0 m bpsl) are drilled from the southern PRD in

Zhuhai, southeast China (Figure 1B). The submarine core P1-1 (79-m-long) was drilled in the Modaomen estuary, and core P3-2 (60-m-long) was drilled in the Zhupai sandbar in the Modaomen Channel. Core P1-1 is composed mainly of a sandy stratum (79.0–58.2 m) and a layer of clay and silt (58.2–0 m). Core P3-2 comprises a basement of dark gray cataclastic breccia and its overlain sediments. The sediments are characterized by a sand layer (53.8–45.8 m) and a succession of clay and silt with sandy laminations (45.8–3.5 m). The top layer of light-yellow silt with plant roots is treated as modern soil (3.5–0 m).

Thirteen OSL samples were collected from cores P1-1 and eight from P3-2. Eight ^{14}C samples were collected from core P3-2. Part of the OSL and AMS ^{14}C data of core P3-2 were reported by Lu et al. (2020) (see Tables 1, 2 for details) to explore regional fault activity.

3 Methods

3.1 OSL dating

3.1.1 Sample preparation and equipment

The outer layer of OSL samples that might have been light-exposed was removed, and the remaining samples were successively treated to remove carbonate and organic matter with 10% HCl and 30% H_2O_2 , respectively. The samples were then wet-sieved to obtain 38–63 or 90–125 μm fractions according to availability. In order to obtain pure quartz OSL grains, the 38–63- μm grains were treated with 35% H_2SiF_6 for

TABLE 1 | Optically stimulated luminescence (OSL) dating results from cores P1-1 and P3-2.

Num.	Sample ID	Depth (m)	Grain size (μm)	Aliquot number	K (%)	Th (ppm)	U (ppm)	Moisture (%)	Dose rate (Gy/ka)	D_e (Gy)	Over-dispersion (%)	OSL age (ka)	References
1	P1-1-1	0.35	90–125	6 ^a +10 ^b	1.58	17.6	3.49	27.1 \pm 5	2.97 \pm 0.10	0.42 \pm 0.04	39.97 \pm 7.20	0.14 \pm 0.02	This study
2	P1-1-2	4.95	90–125	6 ^a +10 ^b	1.67	14.4	3.57	28.4 \pm 5	2.76 \pm 0.10	0.92 \pm 0.05	23.38 \pm 3.79	0.33 \pm 0.03	This study
3	P1-1-9	12.75	90–125	6 ^a +12 ^b	2.06	17	3.31	30.6 \pm 5	3.01 \pm 0.10	1.04 \pm 0.02	6.81 \pm 1.42	0.35 \pm 0.01	This study
4	P1-1-17	27.95	90–125	6 ^a +10 ^b	1.85	18.1	3.21	36.9 \pm 5	2.72 \pm 0.09	9.33 \pm 0.59	27.09 \pm 4.85	3.43 \pm 0.25	This study
5	P1-1-23	42.05	90–125	4 ^a +10 ^b	1.79	16.80	3.40	33.7 \pm 5	2.70 \pm 0.15 ^c	24.71 \pm 1.15	16.34 \pm 3.19	9.15 \pm 0.67	This study
6	P1-1-25	47.05	38–63	6 ^a +12 ^b	1.79	16.80	3.40	32.0 \pm 5	2.80 \pm 0.16 ^c	24.54 \pm 0.37	5.38 \pm 1.14	8.78 \pm 0.51	This study
7	P1-1-27	52.05	90–125	6 ^a +12 ^b	1.79	16.80	3.40	27.2 \pm 5	2.87 \pm 0.16 ^c	29.45 \pm 0.91	11.86 \pm 2.10	10.26 \pm 0.67	This study
8	P1-1-28	54.05	38–63	6 ^a +12 ^b	1.79	16.80	3.40	32.0 \pm 5	2.74 \pm 0.16 ^c	28.57 \pm 0.33	3.82 \pm 1.00	10.41 \pm 0.60	This study
9	P1-1-29	56.05	90–125	6 ^a +12 ^b	1.79	16.80	3.40	28.4 \pm 5	2.89 \pm 0.17 ^c	27.24 \pm 0.56	7.87 \pm 1.48	9.42 \pm 0.57	This study
10	P1-1-30	57.15	90–125	6 ^a +12 ^b	1.79	16.80	3.40	27.8 \pm 5	2.84 \pm 0.16 ^c	28.03 \pm 0.94	13.35 \pm 2.33	9.86 \pm 0.65	This study
11	P1-1-31	58.15	90–125	6 ^a +10 ^b	1.79	16.80	3.40	26.2 \pm 5	2.89 \pm 0.17 ^c	29.48 \pm 1.10	15.31 \pm 2.80	10.19 \pm 0.79	This study
12	P1-1-32	61.2	90–125	6 ^a +12 ^b	1.79	16.80	3.40	30.0 \pm 5	2.79 \pm 0.16 ^c	25.24 \pm 1.03	15.79 \pm 2.81	9.04 \pm 0.63	This study
13	P1-1-34	78.9	90–125	6 ^a +12 ^b	1.79	16.80	3.40	30.0 \pm 5	2.79 \pm 0.16 ^c	22.7 \pm 1.01	19.17 \pm 3.40	8.14 \pm 0.59	This study
14	P3-2-1	4.68	90–125	6 ^a +12 ^b	1.48	11.40	2.32	27.3 \pm 5	2.25 \pm 0.08	0.66 \pm 0.04	24.03 \pm 3.90	0.29 \pm 0.02	Lu et al. (2020)
15	P3-2-2	8.05	90–125	6 ^a +12 ^b	1.15	10.90	2.10	20.6 \pm 5	2.02 \pm 0.08	0.79 \pm 0.04	19.20 \pm 3.01	0.39 \pm 0.02	This study
16	P3-2-3	16.7	90–125	5 ^a +11 ^b	1.40	10.50	2.31	27.9 \pm 5	2.06 \pm 0.08	0.83 \pm 0.04	19.39 \pm 3.45	0.41 \pm 0.02	Lu et al. (2020)
17	P3-2-4	25.3	90–125	6 ^a +12 ^b	1.98	16.50	2.97	32.6 \pm 5	2.80 \pm 0.10	3.93 \pm 0.16	18.11 \pm 2.83	1.41 \pm 0.07	Lu et al. (2020)
18	P3-2-5	32.1	90–125	6 ^a +12 ^b	2.03	16.90	2.82	36.9 \pm 5	2.72 \pm 0.09	17.08 \pm 0.54	12.83 \pm 2.14	6.28 \pm 0.29	Lu et al. (2020)
19	P3-2-6	39.7	90–125	6 ^a +12 ^b	1.93	14.40	2.28	31.8 \pm 5	2.54 \pm 0.09	24.43 \pm 0.80	14.86 \pm 2.33	9.61 \pm 0.46	Lu et al. (2020)
20	P3-2-7	46.6	90–125	6 ^a +11 ^b	1.61	13.24	2.50	25.4 \pm 5	2.42 \pm 0.14 ^c	23.93 \pm 0.49	7.57 \pm 1.48	9.90 \pm 0.62	Lu et al. (2020)
21	P3-2-8	53.8	90–125	6 ^a +11 ^b	1.54	12.93	2.46	28.4 \pm 5	2.28 \pm 0.13 ^c	16.46 \pm 0.65	15.27 \pm 2.72	7.23 \pm 0.51	This study

The superscript “a” means aliquot numbers for single-aliquot regenerative-dose protocol, and the superscript “b” means aliquot numbers for standard growth curve protocol. The superscript “c” represents the dose rates based on the averaged content of U, Th, and K of existing samples.

about 2 weeks, and 90–125- μm grains were etched with 40% HF for 40 min. Both extracted quartz grains were washed with 10% HCl to eliminate fluoride precipitates. The purity of the quartz fractions was tested by OSL IR depletion ratio (Duller, 2003).

OSL measurements were performed on a Risø TL/OSL-DA-20 reader equipped with a $^{90}\text{Sr}/^{90}\text{Y}$ beta source. The quartz OSL signals were stimulated by a blue light ($\lambda = 470 \pm 20 \text{ nm}$) for 40 s

at 130°C and recorded by 9235QA photomultiplier through a 7.5-mm Hoya U-340 filter.

3.1.2 D_e measurements

The equivalent dose (D_e) was determined by a combination of single-aliquot regenerative-dose (SAR) protocol (Murray and Wintle, 2000) and standard growth curve (SGC) protocol (Roberts and Duller, 2004; Lai, 2006; Lai et al., 2007). Yu

TABLE 2 Accelerator mass spectrometry ^{14}C dating results from core P3-2.

Sample ID	Depth (m)	Dating material	^{14}C age (ka BP)	Cal date (2σ) (cal ka BP)	Median cal age(cal ka BP)	References
C-P3-2-1	3.2	Bulk organic	0.59 ± 0.03	0.65–0.58	0.6 ± 0.04	This study
C-P3-2-2	5.2	Plant fragment	0.19 ± 0.03	0.30–0.26	0.3 ± 0.02	Lu et al. (2020)
C-P3-2-3	12.5	Plant fragment	0.21 ± 0.03	0.30–0.27	0.3 ± 0.02	Lu et al. (2020)
C-P3-2-4	21.0	Plant fragment	1.10 ± 0.03	1.06–0.94	1.0 ± 0.07	Lu et al. (2020)
C-P3-2-5	28.0	Plant fragment	7.29 ± 0.03	8.20–8.02	8.1 ± 0.08	Lu et al. (2020)
C-P3-2-6	43.8	Bulk organic	9.21 ± 0.03	10.50–10.46	10.5 ± 0.02	Lu et al. (2020)
C-P3-2-7	45.6	Bulk organic	9.36 ± 0.03	10.66–10.51	10.6 ± 0.08	Lu et al. (2020)
C-P3-2-8	53.6	Plant fragment	9.43 ± 0.04	10.75–10.57	10.7 ± 0.09	Lu et al. (2020)

(2017) and Xu et al. (2020) suggested that it is feasible to choose the preheat temperature of 260°C with a duration of 10 s during the SAR–SGC protocol for dating deltaic samples from the PRD. In this study, a preheat at 260°C for 10 s, and a cut heat at 220°C for 10 s were chosen for regeneration doses and test doses, respectively. For each OSL sample, four to six aliquots were measured by SAR procedures to obtain SAR D_e s and an SGC curve. The other 10–12 aliquots measured for nature signals (L_N/T_N) were fitted in SGC to get the SGC D_e s. The final D_e was calculated using the arithmetic mean.

3.1.3 Dose rate measurements

The U, Th, and K content was determined using neutron activation analysis. The cosmic ray dose was calculated based on altitude, geographical location, and depth of the samples (Prescott and Hutton, 1994). An alpha efficiency factor (a -value) of 0.035 ± 0.003 was used for the 38–63- μm quartz grains (Lai et al., 2008). The water content was measured in the laboratory with an uncertainty of $\pm 5\%$ by considering the seasonal variation of precipitation and the palaeo-climate change in the study area. The D_r s and final ages were calculated on the website program of Dose Rate and Age Calculator (Durcan et al., 2015). Unfortunately, some samples lack measured dose rates due to samples loss. Based on the average value of the available sample data, we calculated the estimated dose rate of these lost samples. The estimated dose rates are generally consistent with the measured dose rates of an upstream core DA (Figure 1B), ranging from 2.09 to 2.92 (Table 1; Xu et al., 2020).

3.2 Radiocarbon dating

Four organic-rich sediments and five plant fragments from core P3-2 were collected for AMS ^{14}C dating. All these AMS ^{14}C samples were analyzed by the Beta Analytic Radiocarbon Dating Laboratory (Florida, USA). All conventional ages were calibrated using Intcal 09 curve (Reimer et al., 2009).

4 Results

4.1 Luminescence characteristics and OSL ages

Figure 2 shows the representative decay and dose–response curves of samples P1-1-17, P1-1-28, P3-2-4, and P3-2-6. The OSL signals of these samples decay rapidly within ~ 2 s, indicating the dominance of the fast component. The SGC can be fitted by a single exponential function with six regenerative dose aliquots, indicating that the SAR–SGC protocol is suitable to determine the D_e values of the PRD sediments.

Thirteen and eight quartz OSL ages are obtained from core P1-1 and P3-2, respectively. The OSL results are listed in Table 1 and shown in Figure 3. The OSL ages range from 10.41 ± 0.60 to 0.16 ± 0.03 ka within depths of 78.90–0.35 m for core P1-1 and from 9.90 ± 0.62 to 0.30 ± 0.02 ka within depths of 4.68–53.80 m for core P3-2 [the dating results were partly from Lu et al. (2020)]. Except for the outlier (the age of 7.05 ± 0.53 ka from the sample P3-2-8), the OSL results are generally consistent with stratigraphic order within errors.

4.2 Radiocarbon ages

The AMS ^{14}C ages of core P3-2 are summarized in Table 2 and Figure 3. The radiocarbon ages of the five plant fragment samples ranged between 10.7 ± 0.09 and 0.3 ± 0.02 cal ka BP within depths of 53.6–5.2 m. The three bulk organic samples yielded ages of 10.60 ± 0.08 cal ka BP (45.6 m), 10.50 ± 0.03 cal ka BP (43.8 m), and 0.06 ± 0.04 cal ka BP (3.2 m) [the dating results are partly from Lu et al. (2020)]. The ^{14}C sample C-P3-2-1 (3.2 m) yielded a slightly older age (0.6 ± 0.04 cal ka BP), which is considered as reworking material because of human re-filling and will not be considered in the sedimentation rate analyses. Except for this sample, the radiocarbon ages of core P3-2 are in agreement with stratigraphic order with depth.

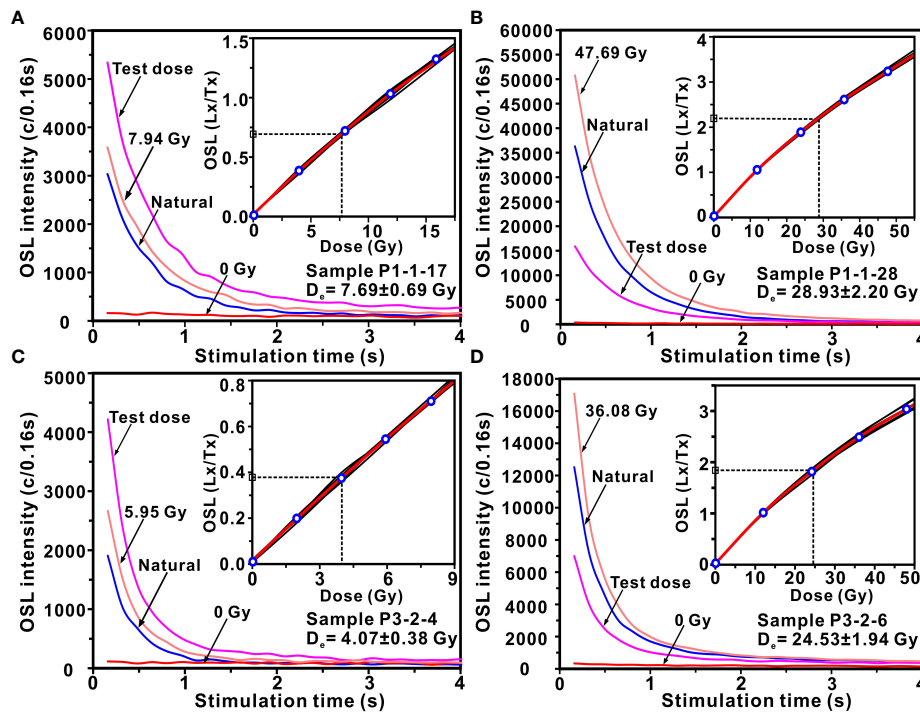


FIGURE 2

Luminescence properties of samples P1-1-17 (A), P1-1-28 (B), P3-2-4 (C), and P3-2-6 (D). The outset figure shows the decay curves of natural signal and the signals of regenerative dose, test dose, and 0 Gy, respectively. The inset figures show the dose–response curves (black lines) of each single-aliquot regenerative-dose aliquot and their standard growth curve (red line). The blue hollow cycles are the regenerative doses.

5 Discussions

5.1 Comparison of OSL and AMS ^{14}C ages

In this study, four quartz OSL ages and three AMS ^{14}C ages of plant fragments show a good agreement above 26 m depth (Figure 4). With increasing depth, the OSL sample P3-2-1 and the ^{14}C sample C-P3-2-2 yielded ages of around 0.3 ka at similar depths (within 0.5 m). The OSL samples P3-2-2, P3-2-3, and P3-2-4 show good constraints for ^{14}C samples C-P3-2-3 and C-P3-2-4 within a range of 0.3 to 1.4 ka. However, the fitting curve show age differences appearing below 26 m in depth, *i.e.*, before 1.4 ka (Figure 4). For instance a c. 2 ka age difference appears between ^{14}C sample C-P3-2-5 (28 m) with an age of 8.1 ± 0.1 cal ka BP and an OSL sample P3-2-5 (32.1 m) with an age of 6.3 ± 0.3 ka. About 30 km north of the study area, core DA revealed a similar age difference by fitting analysis, showing that ^{14}C ages are older (c. 0.5–1 ka) than OSL ages before c. 1.8 ka (Xu et al., 2020). As the depth increases, the age discrepancy of core P3-2 becomes less apparent (Figure 4). For instance at 45.6-m depth, the organic sample C-P3-2-7 (10.6 ± 0.08 cal ka BP) is consistent with the lower OSL sample P-3-2-7 (9.9 ± 0.6 ka) considering age errors.

Comparisons between OSL dating and ^{14}C dating results for Holocene deltaic sediments have been reported in many studies, but their results vary. Research in the eastern PRD showed a good consistency between the Holocene ^{14}C and quartz OSL ages, with only one obviously younger ^{14}C age (Guo et al., 2013). However, as indicated by core DA from the southern PRD, AMS ^{14}C ages are, in general, older than quartz OSL ages for Holocene sediments at similar depths (Xu et al., 2020). The radiocarbon results from the incised valley of the Yangtze River delta likewise showed a good agreement with those in core NT but were mostly older than their corresponding OSL ages in the adjacent core TZ (Nian et al., 2018). Two cores from the Thu Bo River delta in Vietnam revealed a general consistency of quartz OSL and feldspar IR₅₀ ages with ^{14}C ages, except two reversal ^{14}C ages from shell samples in core VG-2 (Qiaola et al., 2022). The causes of these abnormal ^{14}C ages were generally considered as influenced by carbon reservoir effect or the reworking of dating materials (Nian et al., 2018; Xu et al., 2020; Qiaola et al., 2022).

Knowledge of the local surface ocean ^{14}C age offset relative to that of atmospheric CO_2 , the so-called marine reservoir effect (ΔR), is essential for reliable radiocarbon dating of coastal sediments (Stuiver et al., 1986; Stuiver et al., 1998; Southon et al., 2002). During the Holocene, ΔR variations for the South

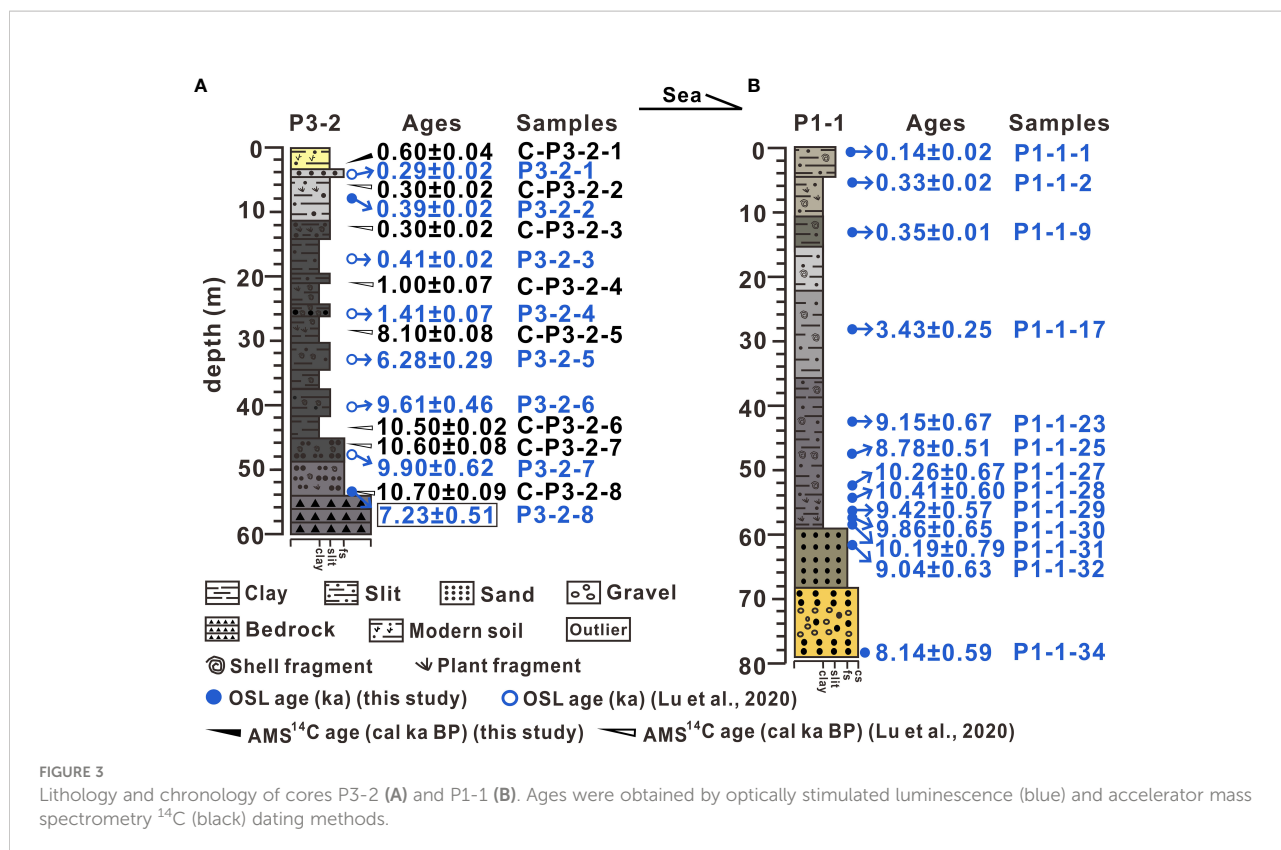


FIGURE 3

Lithology and chronology of cores P3-2 (A) and P1-1 (B). Ages were obtained by optically stimulated luminescence (blue) and accelerator mass spectrometry ¹⁴C (black) dating methods.

China Sea was c. 410 years for c. 8.1–5.5 ka and c. 200 years for c. 3.5–2 ka (Hua et al., 2020). Over the past 500 years, the mean ΔR values for the south/central South China Sea was determined as -25 ± 20 years, while the ΔR values for the South China coast are even lower, between -25 ± 20 and -149 ± 7 years (Southon et al., 2002). In addition to local marine reservoir, calibration of ¹⁴C dating requires analysis of the “dead carbon” effect. For plant samples from drainage systems, the reservoir correction might be higher than that for marine samples due to additional carbonate input from bedrock and soil (Nakanishi et al., 2013). Especially in the carbonated-rich PRD where river flows likely carry old carbon from deeper sediments and sedimentary rocks, the “dead carbon” effect could be more obvious (Liu et al., 2017). For organic matter from the shallow water of the PRD, the high hydrodynamics will produce old carbon and result in abnormally old, by up to 2 ka, ¹⁴C ages (Yim et al., 2006; Kong et al., 2014).

As discussed above, the abnormally older ¹⁴C ages in this study are likely due to the combined effects of regional carbon reservoir and carbon reworking. The mechanisms of the temporal differences in reservoir effects in the PRD, as observed in core P3-2, require further investigation. Considering that deltas are dynamic and actively evolving complex systems, it remains prudent to date Holocene sediments by radiocarbon dating alone.

5.2 Sedimentary units and depositional setting

According to the sedimentary characteristics, the stratigraphic sequences are identified in ascending order of each core (Figure 5). In core P3-2, a 53.8-m-thick Holocene layer consisting of four sedimentary units unconformably overlies the bedrock (dark gray cataclasite and breccia) (Figure 5A). The lowermost unit P3-U1 (53.8–45.8 m) consists of gray-to-dark gray and medium-to-fine sand with few fragments of plant and shell. Such lithology is likely an indication of a tidal channel deposition environment during c. 10.7–9.9 ka. A similar unit was also recorded at around 10.8–10.5 cal ka BP in core ZK19 (31.4–34.8 m in depth) from Lingding Bay (Chen et al., 2019). Unit P3-U2 (45.8–26.1 m) overlies P3-U1 with a mutation in grain size of dark gray muddy clay intercalated with silty-sand laminations and more shell fragments. The lithological transition implies that the depositional setting might have changed from fluvial channel to an estuary/prodelta environment at nearly 10 ka due to sea level rise. Along the Modaomen Channel, a similar sedimentary environmental change was also recorded in upstream cores PRD05, PRD04 (Wei and Wu, 2011), and DA (Xu et al., 2020) during nearly the same time gap (Figure 6). Unit P3-U3 (26.1–11.4 m) shows dark gray muddy silt and sand containing

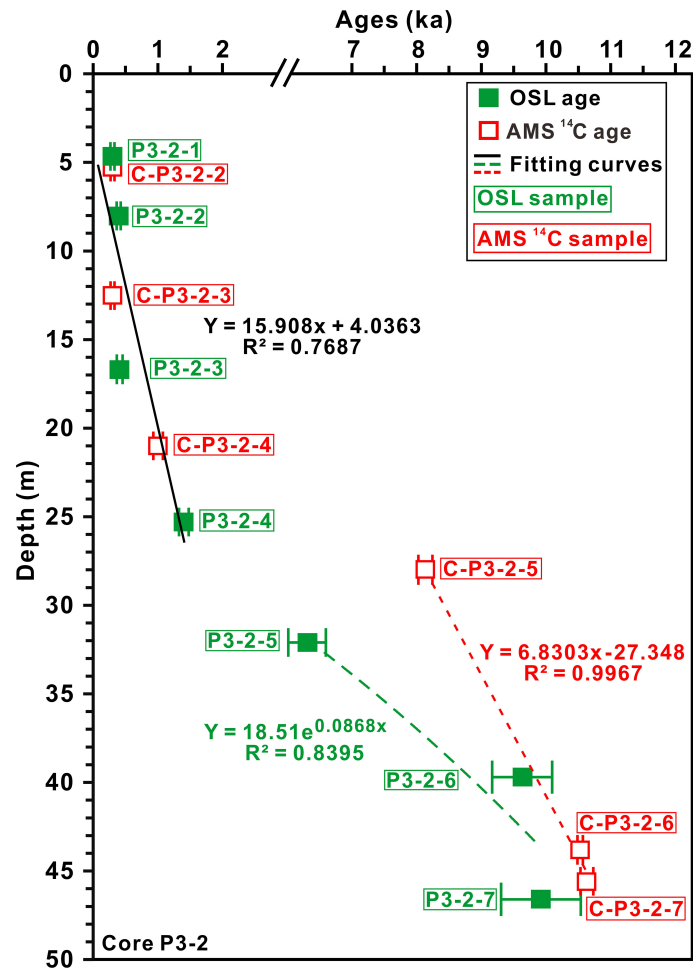
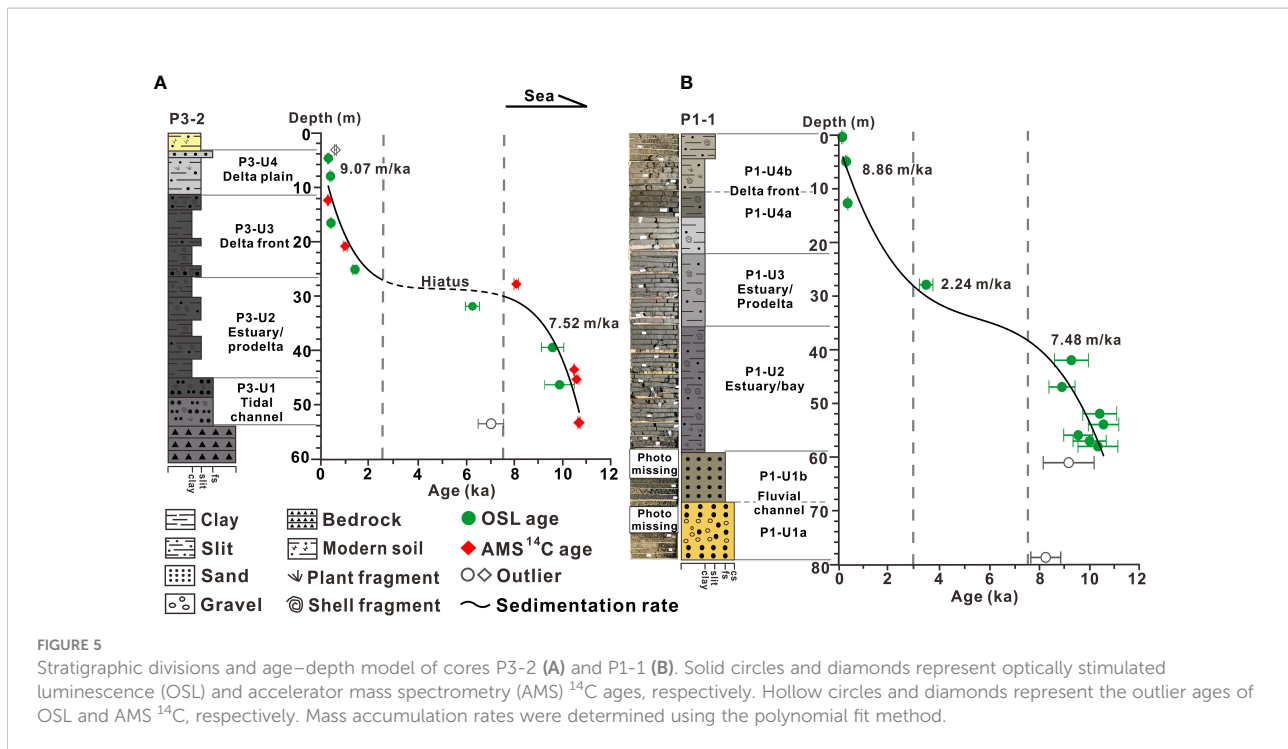


FIGURE 4 Comparison of optically stimulated luminescence (OSL) ages and accelerator mass spectrometry (AMS) ¹⁴C ages of core P3-2 and the fitting curves for these ages. Circles and diamonds represent OSL and AMS ¹⁴C ages, respectively. Ages above 26 m in depth are well fitted by a linear function (black). Below 26 m in depth, OSL and AMS ¹⁴C were fitted by an exponential (green) and a linear function (red), respectively.

abundant shell fragments and coarse sand laminations at the bottom and fine sand laminations at depths of 14.0–11.4 m. The uppermost P3-U4 (11.4–3.5 m) is mainly composed of light gray silt with sporadic fine sandier lenses and a thin sandy layer (5.0–3.5 m). The upward fining-to-coarsening successions and sandier lenses indicate that this site might be deposited in a delta front (P3-U3) to a delta plain (P3-U4) setting (Figure 5A).

Core P1-1 is divided into four units (Figure 5B). The basal unit P1-U1 consists of two subunits. The lower unit P1-U1a (79–68 m) is an 11-m-thick layer of brownish-yellow coarse sand with well-rounded and poorly sorted grave sediments, and the upper unit P1-U1b (68.0–58.2 m) is grayish-yellow medium-to-fine sand. Unit P1-U1 is interpreted as indicating a fluvial channel environment. Unit P1-U2 (58.2–36.0 m) is unconformably in contact with the underlying strata with mutation in color and grain size, consisting of the dark gray

color of silty clay, including abundant fragments of oyster shells and plant. The lithologic characteristics of this unit shows a similarity to P3-U2 and is considered as estuarine/bay deposits (Figure 5). This unit was also documented at depths of c. 51–32 m in the adjacent core ZK2, which has been interpreted as retrogradational estuary since c. 7.5 ka (Wei and Wu, 2011). Unit P1-U3 (36.0–22.0 m) appears as a continuous depositional succession of unit P1-U2 with gradual contact, composed of gray silty clay sediments with fewer shell fragments. Unit P1-U4 (22–0 m) occupies the uppermost part of core P1-1 with two subunits. The lower unit P1-U4a (22–16 m) is light gray clay sediments. The upper unit P1-U4b (16–0 m) consists of grayish-brown to brownish-gray clay and sandy silt with organic muddy sediments and a few plant fragments. The upward-coarsening trend and fewer shell fragments compared with P1-U2 probably represent a



transition from estuarine/prodelta (P1-U3) to delta front (P1-U4) environment.

In the present study, unit P1-U1 was subjected to a different depositional system (fluvial system) compared to other units in core P1-1 (Figure 5B) and is excluded from the sedimentation rate analysis. In both cores P3-2 and P1-1, three phases of depositional rate changes are identified based on the obtained ages (Figure 5). During 10.7–7.5 ka, cores P3-2 and P1-1 deposited at a rate of 7.52 and 7.48 m/ka, respectively. Between 7.5 and 2.5 ka, core P3-2 appeared as a sedimentary hiatus, whereas core P1-1 recorded a slow accumulation of 2.24 m/ka from 7.5 to 3.0 ka. The highest accumulation rate is recorded since 3 ka as c. 9.07 m/ka in core P3-2 and 8.86 m/ka in core P1-1.

5.3 Variation of sedimentation rates and its evolutionary implication for the Pearl River Delta

5.3.1 Rapid sea level rise and accommodation space infilling

Theoretically, one (or more) sequence(s) of marine sediments can be found within a tectonically subsiding delta basin and its incision valley systems due to sea level changes during glacial-interglacial cycles (Dalrymple et al., 1992; Zaitlin et al., 1994; Nichol et al., 1996). Previous studies have shown that at least two marine sequences have been consistently recorded

along the northern coast of the South China Sea during the Quaternary period (Huang et al., 1982; Yim et al., 2008; Zong et al., 2009b; Xu et al., 2022). As indicated by the Quaternary sedimentary record from the PRD, the catchment area was filled with older marine sediments that may have been deposited during MIS 5 (Yim et al., 1990; Zong et al., 2009b; Yu, 2017) as well as fluvial sands and gravels. This older sedimentary succession is generally overlain bedrock or gravel beds in the coastal areas of southern China (Zong et al., 2015). Since the LGM, when the sea level dropped to about 120 m bpsl (Chappell et al., 1996), the Pearl River cut through the older succession and created incised channels (Figure 7A; Zong et al., 2009b). Along with sea level that reached to about 40 m bpsl at c. 10 cal ka BP (Siddall et al., 2003; Xiong et al., 2018b), available space was created at many locations along the coast that would be filled during the Holocene (e.g., Zong et al., 2012).

When the relative sea level in the study area rose from about 40 to 0 m bpsl between c. 10 and 7.5 ka (e.g., Xiong et al., 2018b), seawater inundated the study area and transformed it into a broad estuary (Figure 7B). At the same time, units P1-U2 and P3-U1 deposited in an estuary environment at high accumulation rates of 7.47 m/ka in core P1-1 and 7.39 m/ka in core P3-2 (Figure 5). This rapid sedimentation during the early Holocene has been widely reported from the head (e.g., Zong et al., 2009a; Fu et al., 2020), central deltaic plain (Zhao et al., 2014; Fu et al., 2020), and estuarine areas (Chen et al., 2019) in the context of rising sea level. Previous studies showed that the rate of relative sea level rise increased from about 16.4 m/ka by

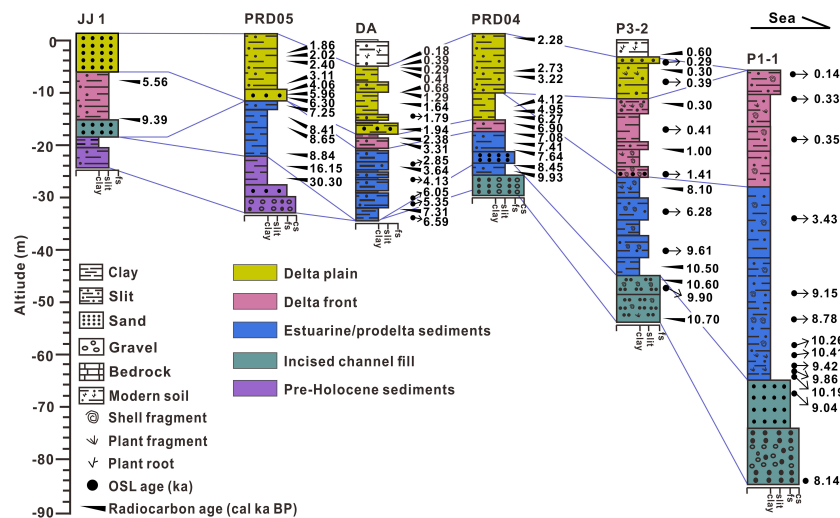


FIGURE 6

Stratigraphic transect along the palaeo-valley from central deltaic plain to the Modaomen estuary showing the distribution of major sediment facies and the seaward-thickening Holocene stratum. The stratigraphic analyses of cores were cited from previous studies, *i.e.*, JJ1 by Zong et al. (2009a), PRD05 by Liu et al. (2008), DA by Xu et al. (2020), and PRD04 by Wei and Wu (2011).

10.5 cal ka BP to a peak of c. 33.0 m/ka by 9.5 cal ka BP (Xiong et al., 2018b). As the seaward part of the delta, an estuarine area would respond immediately to rapid sea level rise, opening a narrow accommodation space for fast infilling of incision channels (Chen et al., 2019).

5.3.2 Slow sedimentation in the middle Holocene

As the relative sea level approximately ceased rising around 7.5 cal ka BP at a reduced rate of 1.7 m/ka (Xiong et al., 2018b), core P1-1 experienced a markedly slow deposition at 2.24 m/ka between 7.5 and 3.0 ka (Figure 5B). This slow sedimentation rate during the middle Holocene has been recorded in many boreholes from the PRD (Zong et al., 2009a; Hu et al., 2013; Liu et al., 2016; Fu et al., 2020). The reasons for this phenomenon are argued as follows: (1) low sediment supply as sedimentation was concentrated in the head area (Fu et al., 2020), (2) less sediment generation under the influence of the weakening summer monsoon (Zong et al., 2006), and (3) strong tidal currents that transported parts of suspended sediments into the South China Sea (Wu et al., 2007). Consequently, limited sediments entered the estuary and were frequently reworked by tidal currents. However, small and large former/present rocky islands across the estuary of the PRD may have contributed to the trapping of sediments to its adjacent areas (Huang et al., 1982; Wu et al., 2007; Fu et al., 2020). For example, in the bay area, core HKUV11 near Lantau Island (Hong Kong) recorded continuous sedimentation (1.8 m/ka) over the last 8 ka (Xiong et al., 2018b). Therefore, despite the low sediment supply from the PRD, Hengqin Island, adjacent to core

P1-1 (Figure 1B), may have supplied some sediment flux and contributed to the formation of unit P1-U3 (36.0–23.0 m) during 7.5–3.0 ka (Figure 5).

However, core P3-2, located about 20 km upstream of core P1-1, underwent an exceptionally low depositional rate of 0.7 m/ka from 7.5 to 2.5 ka. This rate is much lower than that of downstream core P1-1 (2.24 m/ka) during 7.5–3.0 ka (Figure 5) and also those (1.27–5.66 m/ka) in modern PRD estuaries (Liu et al., 2014). Here the slow sedimentation process is interpreted as a depositional hiatus during the middle Holocene (Figure 5A). In Lingding Bay, sedimentary hiatuses from 8.1 to 2.2 cal ka BP and from 7.6 to 2.9 cal ka BP were also reported for cores ZK19 and ZK13, respectively (Chen et al., 2019). In these cores, the palaeo-morphology of the PRD is suggested as a key factor of the hiatuses (Chen et al., 2019). Core P3-2 is located in the Modaomen Channel and is surrounded by mountains (*e.g.*, Wugui Mountains) and rocky islands (Figures 1B, 7B), where a special hydrology called tidal bi-directional jet flows (TBJFs) likely developed as the extensive transgression passed through (Wu et al., 2010). However, core P1-1 is located in the mouth of the Modaomen estuary, where tidal currents are more complex and exhibit significant dissipation of tidal energy. Such a turbulent environment is unfavorable for the existence of TBJFs (Wei et al., 2011). Recent studies reported that the TBJFs enhanced seafloor erosion in the tidal channel with strong influx and convergence of palaeo-tidal energy (Wu et al., 2010; Wei and Wu, 2014). A long-term morphodynamic model simulated the tidal current velocity in the PRD, showing that the highest

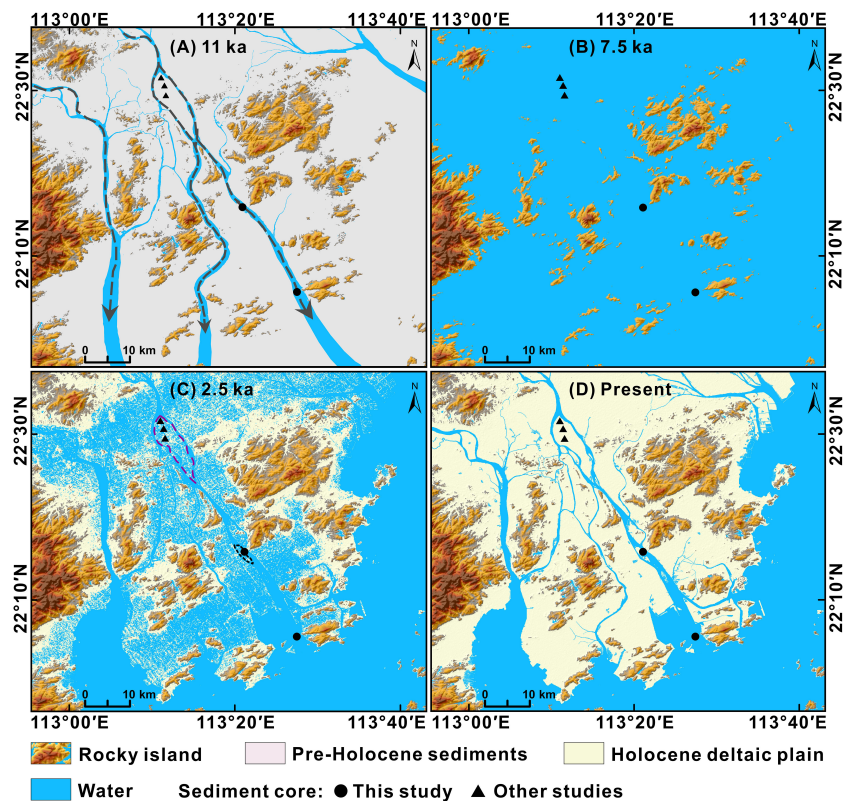


FIGURE 7

Changes of landscapes of the southern Pearl River Delta estuary during the Holocene. (A) Prior to the Holocene marine transgression, the fluvial forces (gray dotted arrows) created incised valleys and cut through pre-Holocene sediments. (B) Stage I occurred at the maximum transgressive invasion at c. 7.5 ka when seawater flooded the study area and turned it into estuarine condition, with only rocky islands emerging. (C) Stage II took place during marine regression when progradation of deltaic plain started since c. 2.5 ka, with sporadic wetlands. The dotted lines represent the developing formation of Daao sandbar (in purple) and Zhupai sandbar (in black). (D) In stage III of the past 2.5 ka, the Daao sandbar and Zhupai sandbar had already formed under rapid sedimentation rates. The black dots show the locations of the sediment cores by this study, with black triangles as those proposed by Liu et al. (2008); Xu et al. (2020), and Wei et al. (2011) from north to south, respectively.

velocity is distributed in the southwest side of Wugui Mountains from 6.0 to 2.5 ka (Wu et al., 2010). In core P3-2, such a strong hydrodynamic condition is characterized as plenty of coarse sand and shell fragments at depths of 26.1–26.3 m (Figure 3A). Together with the low sediment supply, core P3-2 has closely ceased deposition since 7.5 ka.

5.3.3 Accelerated sedimentation and formation of the deltaic plain

The slow sedimentation rate transitioned to rapid deposition (c. 9 m/ka) as observed in both cores in 2.5 ka (Figure 5). Extremely rapid deposition became a major feature of the PRD in a period of relative sea level stability during the late Holocene (Zong et al., 2010). As the central basin was gradually filled between c. 4 and 2 ka (Fu et al., 2020), the deltaic progradation shifted to the estuary area since c. 2.5 ka (Figure 7C), and the sedimentation rate was up to 5.33 m/ka, on average, for the Modaomen estuary (Wei et al., 2011). Human activities, such as

catchment land clearance, diking, and reclamation, have been intensified since c. 2.2 ka (Cheng et al., 2018; Xiong et al., 2020; Chen et al., 2022), causing increased soil erosion (Yu et al., 2010; Hu et al., 2013; Zong et al., 2013; Zheng et al., 2021) and more sediment trapping (Figure 7C; Zong et al., 2009a; Xiong et al., 2020). In the estuary, cores B1/2 and HKUV1 showed that the progressively higher kaolinite contents since 2.5 ka were due to older weathered soils caused by widespread agriculture (Hu et al., 2013); core ZK19 showed a strengthening of anthropogenic influence, as evidenced by gradually positive $\delta^{13}\text{C}$ values at depths of 9.8–0 m (gray to brown and gray clayey silt) since c. 1.7 ka (Chen et al., 2019). A similar lithology was also recorded in unit P1-U4b (grayish brown to brownish gray, clay and silty sand) at the same time (Figure 5B). Therefore, the fast deposition in core P1-1 could be associated with intense human activities.

After c. 2.5 ka, the TBJFs has switched into a unidirectional jet flow with weakened tidal energy (Wu et al., 2010; Wu and

Wei, 2021), and thus sedimentation of core P3-2 in the Modaomen Channel is likely reactivated. Based on the records of cores PRD04 and PRD05, the tidal sand bodies of the Modaomen Channel were aerial in origin and formed sandbars (e.g., Daao sandbar; Figure 7C) at c. 2.2 ka (He et al., 2007; Wei and Wu, 2011). About 34 km downstream from core PRD05, units P3-U3 and P3-U4 consist of coarsening upward sediments near the land surface, implying that core P3-2 had gradually switched from the underwater sand body to the modern deltaic floodplain (Zhupai sandbar; Figures 5A, 7C, D). Xu et al. (2020) suggested that the Modaomen estuary changed from a relatively open estuarine bay to a relatively closed one at 2 ka, which caused the reduction in outward sediment flux and trapping of a large amount of sediment. Hence, the rapid sedimentation in core P3-2 is more likely to be controlled by the weakening tidal process.

5.4 Comparison with other Asian megadeltas

The three-stage sedimentation model proposed in this study has also been recorded in many Asian deltas. For instance the high sediment accumulation rates in the Yangtze River delta vary between c. 4.2 and 10.0 m/ka during the early Holocene (c. 10–7 ka) (Nian et al., 2018; Wang et al., 2018; Jiang et al., 2020). In addition, in the Mekong River delta, a c. 20-m-thick layer of marine and brackish-water sediments were deposited in a short time period of 11.6–9.1 cal ka BP (Tamura et al., 2012). A similar sequence has also been recorded in the southern Ganges–Brahmaputra delta (Goodbred and Kuehl, 2000) and the Song Hong delta (Tanabe et al., 2006). Subsequently during c. 7–2 ka, the sedimentation rate was less than 5 m/ka, on average, in the Yangtze River delta, possibly because of the migration of the depo-center (Nian et al., 2018; Wang et al., 2018; Jiang et al., 2020). In the Mekong River delta, the accumulation rate significantly slowed down to 0.3–0.7 m/ka, which was associated with the lateral switching of distributary channels (Tamura et al., 2009; Tamura et al., 2012). The delta front progradation rate at 10 m bpsl also decelerated from 22 to 4 m/a in the Song Hong delta at c. 6 cal ka BP (Tanabe et al., 2006). In the last 2 ka, accelerated sedimentation and rapid coastline advances occurred in the Yangtze River and Mekong River deltas due to the gradual seaward shift of sandy shoals and bars (Tamura et al., 2012; Wang et al., 2018; Jiang et al., 2020).

Though under common monsoon climate and sea level histories, differences still exist in Asian megadeltas on their sedimentary characteristics. In contrast to the broad channel of the Yangtze River delta (60–70-km-wide in the estuary; Li et al., 2002), the palaeo-incised valley of the PRD is tight [30–60-km-wide for the central basin and estuarine bay; from

Zong et al. (2012)]. In addition, the Holocene strata of the PRD show a trend of gradual thickening from the central deltaic plain to the estuary (Figure 6), with an average of about 20 m and more than 25 m in palaeo-incised valleys (Huang et al., 1982; Zong et al., 2009a). Nevertheless, cores P1-1 and P3-2 show remarkably thicker Holocene sediments (c. 79 and 54 m, respectively), which might be related to differences in palaeo-topography. The narrower and seaward deepening estuarine channel may have amplified the effects of monsoonal fluvial processes on the evolution of the estuarine-deltaic landscape during the early Holocene (Zong et al., 2012). Strong fluvial forcing was recorded at c. 10.6–9.6 ka in cores HKUV12 and HKUV10 along a palaeo-incised channel of Lantau Island, supported by a low abundance of brackish diatoms and high TOC content from terrigenous materials (Xiong et al., 2018a). Compared with tidal-dominated silt and clay deposited contemporaneously in other Asian deltas (Goodbred and Kuehl, 2000; Tamura et al., 2012; Wang et al., 2018), unit 1 (early-Holocene sequence) of cores P1-1 and P3-2 is dominated by sands (Figure 5), also implying a possible link to the strong fluvial influence.

Conclusions

In this study, cores P1-1 and P3-2 were drilled in the Southern PRD for OSL and AMS ¹⁴C dating. The chronology of core P1-1 ranging from 10.4 to 0.16 ka is obtained from 13 quartz OSL ages. Core P3-2 spans from 10.7 to 0.3 ka, including eight OSL ages and eight AMS ¹⁴C ages. The OSL and ¹⁴C data shows a good consistency above 26 m (1.4–0.3 ka), but with differences at depths of 26–54 m where AMS ¹⁴C ages (8.1–10.7 ka) are, in general, older (up to c. 2 ka) than quartz OSL ages. This discrepancy decreases with depths. Therefore, one should remain cautious when dating Holocene sediments by only radiocarbon dating.

The obtained chronostratigraphy reveals three stages of sedimentation: (1) high accumulation rates of 7.48 (P1-1) and 7.52 (P3-2) m/ka between c. 10.7 and 7.5 ka as a result of rapid marine transgression, (2) followed by an exceptionally decreasing rate 2.24 m/ka (P1-1) and a sedimentary hiatus (P3-2) during c. 7.5–2.5 ka as most sediments were trapped in the head area and due to strong scouring by tidal forces in the estuary, and (3) rapid sedimentation at a rate of c. 9 m/ka since c. 2.5 ka, which was related to intensive human activities and weakening tidal hydrodynamics.

This sedimentary model is also evident in other Asian deltas. However, differences still exist due to the unique palaeo-morphology of the PRD. The narrower and seaward deepening estuarine channel may have led to the stronger fluvial influence during the early Holocene.

Data availability statement

The original contributions presented in the study are included in the article/supplementary material. Further inquiries can be directed to the corresponding authors.

Author contributions

ZL organized the work. PL, XX, and ZL wrote the original draft. YC and PL measured the optically stimulated luminescence samples in the laboratory. MA revised and helped to improve the manuscript. PL, YC, XX, and ZL analyzed the data. ZL and LL collected the samples during drilling. All authors contributed to the article and approved the submitted version.

Funding

This research was supported by STU Scientific Research Start-Up Foundation for Talents (NTF19003 and NTF20006), and Innovation and Entrepreneurship Project of Shantou (2021112176541391).

References

- Bianchi, T. S., and Allison, M. A. (2009). Large-River delta-front estuaries as natural "recorders" of global environmental change. *Proc. Natl. Acad. Sci. U.S.A.* 106 (20), 8085–8092. doi: 10.1073/pnas.0812878106
- Chappell, J., Omura, A., Esat, T., McCulloch, M., Pandolfi, J., Yoko, O., et al. (1996). Reconciliation of late quaternary Sea levels derived from coral terraces at huon peninsula with deep Sea oxygen records. *Earth Planet Sci. Lett.* 144 (1), 227–236.
- Cheng, Z., Weng, C., Steinke, S., and Mohtadi, M. (2018). Anthropogenic modification of vegetated landscapes in southern China from 6,000 years ago. *Nat. Geosci.* 11 (12), 939–943. doi: 10.1038/s41561-018-0250-1
- Chen, X., Huang, X., Wu, D., Chen, J., Zhang, J., Zhou, A., et al. (2022). Late Holocene land use evolution and vegetation response to climate change in the watershed of xingyun lake, SW China. *Catena* 211. doi: 10.1016/j.catena.2021.105973
- Chen, H. X., Wang, J. H., Khan, N. S., Waxy, L. L., Wu, J. X., Zhai, Y. H., et al. (2019). Early and late Holocene paleoenvironmental reconstruction of the pearl river estuary, south China Sea using foraminiferal assemblages and stable carbon isotopes. *Estua. Coast. Shelf. Sci.* 222, 112–125. doi: 10.1016/j.ecss.2019.04.002
- Dalrymple, R. W., Zaitlin, B. A., and Boyd, R. (1992). Estuarine facies models: conceptual basis and stratigraphic implications. *J. Sediment. Res.* 62 (6), 1130–1146. doi: 10.1306/d4267a69-2b26-11d7-8648000102c1865d
- Duller, G. A. T. (2003). Distinguishing quartz and feldspar in single grain luminescence measurements. *Radiat. Measure.* 37 (2), 161–165. doi: 10.1016/s1350-4487(02)00170-1
- Durcan, J. A., King, G. E., and Duller, G. A. T. (2015). DRAC: Dose rate and age calculator for trapped charge dating. *Quatern. Geochronol.* 28, 54–61. doi: 10.1016/j.quageo.2015.03.012
- Fu, S. Q., Xiong, H. X., Zong, Y. Q., and Huang, G. Q. (2020). Reasons for the low sedimentation and slow progradation in the pearl river delta, southern China, during the middle Holocene. *Mar. Geol.* 423. doi: 10.1016/j.margeo.2020.106133
- Fyfe, J. A., Selby, I. C., Shaw, R., James, J. W. C., and Evans, C. D. R. (1997). Quaternary sea-level change on the continental shelf of Hong Kong. *J. Geol. Soc.* 154 (6), 1031–1038. doi: 10.1144/gsjgs.154.6.1031
- Gao, L., Long, H., Shen, J., Yu, G., and Yin, Y. (2016). High-resolution OSL dating of a coastal sediment sequence from the south yellow Sea. *Geochronometria* 43 (1), 143–154. doi: 10.1515/geochr-2015-0044
- Goodbred, S. L., and Kuehl, S. A. (2000). The significance of large sediment supply, active tectonism, and eustasy on margin sequence development: Late quaternary stratigraphy and evolution of the Ganges–Brahmaputra delta. *Sediment. Geol.* 133 (3–4), 227–248. doi: 10.1016/s0037-0738(00)00041-5
- Guo, L. T., Wang, P., Zhang, K., Sheng, Q., Zhao, H., and Wang, C. M. (2013). OSL and 14C ages of the late quaternary sediments in the east pearl river delta (in Chinese with English abstract). *Geol. China* 40 (6), 1842–1849.
- He, J., Garzanti, E., Cao, L. C., and Wang, H. (2020). The zircon story of the pearl river (China) from Cretaceous to present. *Earth-Sci. Rev.* 201. doi: 10.1016/j.earscirev.2019.103078
- He, Y., Liu, X. J., Duan, Z. H., Liu, C., Hou, P., Lu, C., et al. (2022). Long-term morphodynamic evolution in the modaomen estuary of the pearl river delta, south China. *Geomorphology* 398. doi: 10.1016/j.geomorph.2021.108057
- He, Z., Mo, W., Liu, C., and Wu, J. C. (2007). Formation of xijiang daao sha in pearl river delta during the postglacial period from a perspective of sedimentation rates and sediment grain size (in Chinese with English abstract). *J. Palaeogeogr.* 9 (3), 331–336. doi: 10.3969/j.issn.1671-1505.2007.03.011
- Hori, K., and Saito, Y. (2007). An early Holocene sea-level jump and delta initiation. *Geophys. Res. Lett.* 34 (18). doi: 10.1029/2007gl031029
- Hori, K., Saito, Y., Zhao, Q. H., and Wang, P. X. (2002). Architecture and evolution of the tide-dominated changjiang (Yangtze) river delta, China. *Sediment. Geol.* 146 (3–4), 249–264. doi: 10.1016/s0037-0738(01)00122-1
- Hua, Q., Ulm, S., Yu, L., Clark, T. R., Nothdurft, L. D., Leonard, N. D., et al. (2020). Temporal variability in the Holocene marine radiocarbon reservoir effect for the Tropical and South Pacific. *Quaternary Sci. Rev.* 249. doi: 10.1016/j.quascirev.2020.106613
- Huang, Z. G., Li, P. R., Zhang, Z. Y., Li, K. H., and Qiao, P. N. (1982). *The formation and evolution of pearl river delta* (Guangzhou: Science Populariazaiton Press).
- Hu, D. K., Clift, P. D., Böning, P., Hannigan, R., Hillier, S., Blusztajn, J., et al. (2013). Holocene Evolution in weathering and erosion patterns in the pearl river delta. *Geochem. Geophys. Geosyst.* 14 (7), 2349–2368. doi: 10.1002/ggge.20166
- Jiang, F., Zhao, X. S., Chen, J., Liu, Y., Sun, Q. L., Chen, J., et al. (2020). Depocenter shift and en-echelon shoal development in the pre-Holocene incised valley of the Yangtze delta, China. *Mar. Geol.* 426. doi: 10.1016/j.margeo.2020.106212

Acknowledgments

We thank Chang Huang of Hong Kong University and Ping Wang of China Earthquake Administration for help in the field work.

Conflict of interest

The authors declare that the research was conducted in the absence of any commercial or financial relationships that could be construed as a potential conflict of interest.

Publisher's note

All claims expressed in this article are solely those of the authors and do not necessarily represent those of their affiliated organizations, or those of the publisher, the editors and the reviewers. Any product that may be evaluated in this article, or claim that may be made by its manufacturer, is not guaranteed or endorsed by the publisher.

- Kong, D. M., Zong, Y. Q., Jia, G. D., Wei, G. J., Chen, M. T., and Liu, Z. H. (2014). The development of late Holocene coastal cooling in the northern south China Sea. *Quatern. Int.* 349, 300–307. doi: 10.1016/j.quaint.2013.08.055
- Lai, Z. P. (2006). Testing the use of an OSL standardised growth curve (SGC) for determination on quartz from the Chinese loess plateau. *Radiat. Measure.* 41 (1), 9–16. doi: 10.1016/j.radmeas.2005.06.031
- Lai, Z. P., Wintle, A. G., and Thomas, D. S. G. (2007). Rates of dust deposition between 50 ka and 20 ka revealed by OSL dating at yuanbao on the Chinese loess plateau. *Palaeogeogr. Palaeoclimatol. Palaeoecol.* 248 (3–4), 431–439. doi: 10.1016/j.palaeo.2006.12.013
- Lai, Z. P., Zöller, L., Fuchs, M., and Brückner, H. (2008). Alpha efficiency determination for OSL of quartz extracted from Chinese loess. *Radiat. Measure.* 43 (2–6), 767–770. doi: 10.1016/j.radmeas.2008.01.022
- Li, P. R., Lin, X. D., and Huang, G. Q. (1991). Geomorphological characteristics and development in East river delta (in Chinese with English abstract). *Geo. Res.* 10 (2).
- Li, C., Wang, P., Sun, H., Zhang, J., Fan, D., and Deng, B. (2002). Late Quaternary incised-valley fill of the Yangtze delta (China): its stratigraphic framework and evolution. *Sedimentary Geology* 152 (1–2), 133–158. doi: 10.1016/s0037-0738(02)00066-0
- Liu, Y. L., Gao, S., Wang, Y. P., Yang, Y., Long, J. P., Zhang, Y. Z., et al. (2014). Distal mud deposits associated with the pearl river over the northwestern continental shelf of the south China Sea. *Mar. Geol.* 347, 43–57. doi: 10.1016/j.margeo.2013.10.012
- Liu, C. L., TFursich, F., Dong, Y. X., Che, X. G., Chen, L., and Zhuang, C. (2008). High resolution ostracod records of borehole PRD05 and the late quaternary palaeoenvironment in the pearl river delta (in Chinese with English abstract). *J. Palaeogeogr.* 10 (3), 313–322.
- Liu, C. Y., Yin, J., Liu, C. L., Huang, Y., and Wu, Y. Q. (2016). Holocene Mollusc records and palaeoenvironmental changes in the pearl river delta (in Chinese with English abstract). *Trop. Geogr.* 36 (3), 355–363. doi: 10.13284/j.cnki.rddl.002830
- Liu, Z. H., Zhao, M., Sun, H. L., Yang, R., Chen, B., Yang, M. X., et al. (2017). “Old” carbon entering the south China Sea from the carbonate-rich pearl river basin: Coupled action of carbonate weathering and aquatic photosynthesis. *Appl. Geochem.* 78, 96–104. doi: 10.1016/j.apgeochem.2016.12.014
- Long, Z. R., Wang, Z. B., Tu, H., Li, R. H., Wen, Z. H., Wang, Y. X., et al. (2022). OSL and radiocarbon dating of a core from the bohai Sea in China and implication for late quaternary transgression pattern. *Quatern. Geochronol.* 70. doi: 10.1016/j.quageo.2022.101308
- Lu, B. H., Wang, P., Wang, H. Y., Lai, Z. P., Deng, Z. H., Bi, L. S., et al. (2020). Latest progress on activity of heshan-modaomen segment, xijiang fault. *Seismol. Geol.* 42 (6), 1370–1384. doi: 10.3969/j.issn.0253-4967.2020.06.007
- McLean, R. F., and Tsyban, A. (2001). “Coastal zones and marine ecosystems,” in *Climate change 2001: impacts, adaptation, and vulnerability*. Eds. J. J. Carthy, O. F. Canziani, N. A. Leary, D. J. Dokken and K. S. White (London: Cambridge University Press), 343–379.
- Murray, A. S., and Wintle, A. G. (2000). Luminescence dating of quartz using an improved single-aliquot regenerative-dose protocol. *Radiat. Measure.* 32 (1), 57–73. doi: 10.1016/s1350-4487(99)00253-x
- Nakanishi, T., Hong, W., Sung, K. S., and Lim, J. (2013). Radiocarbon reservoir effect from shell and plant pairs in Holocene sediments around the yeongsan river in Korea. *Nucl. Instruments Methods Phys. Res. Section B: Beam Interact. Materials Atoms* 294, 444–451. doi: 10.1016/j.nimb.2012.09.025
- Nian, X., Zhang, W., Wang, Z., Sun, Q., and Chen, Z. (2021). Inter-comparison of optically stimulated luminescence (OSL) ages between different fractions of Holocene deposits from the Yangtze delta and its environmental implications. *Mar. Geol.* 432. doi: 10.1016/j.margeo.2020.106401
- Nian, X. M., Zhang, W. G., Wang, Z. H., Sun, Q. L., Chen, J., and Chen, Z. Y. (2018). Optical dating of Holocene sediments from the Yangtze river (Changjiang) delta, China. *Quatern. Int.* 467, 251–263. doi: 10.1016/j.quaint.2018.01.011
- Nichol, S. L., Boyd, R., and Penland, S. (1996). Sequence stratigraphy of a coastal-plain incised valley estuary: Lake calcasieu, Louisiana. *J. Sediment. Res.* 66. doi: 10.1306/d426841e-2b26-11d7-8648000102c1865d
- Owen, R. B., Neller, R. J., Shaw, R., and Cheung, P. C. T. (1998). Late quaternary environmental changes in Hong Kong. *Palaeogeogr. Palaeoclimatol. Palaeoecol.* 138 (1–4), 151–173. doi: 10.1016/s0031-0182(97)00129-6
- Prescott, J. R., and Hutton, J. T. (1994). Cosmic ray contributions to dose rates for luminescence and ESR dating: Large depths and long-term time variations. *Radiat. Measure.* 23 (2–3), 497–500. doi: 10.1016/1350-4487(94)90086-8
- Qiaola, S., Nguyen, T. M. L., Ta, T. K. O., Nguyen, V. L., Gugliotta, M., Saito, Y., et al. (2022). Luminescence dating of Holocene sediment cores from a wave-dominated and mountainous river delta in central Vietnam. *Quatern. Geochronol.* 70. doi: 10.1016/j.quageo.2022.101277
- Reimer, P. J., Baillie, M. G. L., Bard, E., and Bayliss, A. (2009). INTCAL09 and Marine09 radiocarbon age calibration curves, 0–50000 years. *Radiocarbon* 51 (4), 1111–1150. doi: 10.1017/S0033822200048864
- Roberts, H. M., and Duller, G. A. T. (2004). Standardised growth curves for optical dating of sediment using multiple-grain aliquots. *Radiat. Measure.* 38 (2), 241–252. doi: 10.1016/j.radmeas.2003.10.001
- Saito, Y., Katayama, H., Ikehara, K., Kato, Y., Matsumoto, E., Oguri, K., et al. (1998). Transgressive and highstand systems tracts and post-glacial transgression, the East China Sea. *Sediment. Geol.* 122 (1–4), 217–232. doi: 10.1016/s0037-0738(98)00107-9
- Saito, Y., Yang, Z. S., and Hori, K. (2001). The huanghe (Yellow river) and changjiang (Yangtze river) deltas: a review on their characteristics, evolution and sediment discharge during the Holocene. *Geomorphology* 41 (2–3), 219–231. doi: 10.1016/s0169-555x(01)00118-0
- Siddall, M., Rohling, E. J., Almogi-Labin, A., Hemleben, C., Meischner, D., Schmelzer, I., et al. (2003). Sea-level fluctuations during the last glacial cycle. *Nature* 423 (6942), 853–858. doi: 10.1038/nature01690
- Southon, J., Kashgarian, M., Fontugne, M., Metivier, B., and W-S Yim, W. (2002). Marine reservoir corrections for the Indian ocean and southeast Asia. *Radiocarbon* 44 (1), 167–180. doi: 10.1017/s0033822200064778
- Stanley, D. J., and Warne, A. G. (1994). Worldwide initiation of holocene marine deltas by deceleration of sea-level rise. *Science* 265 (5169), 228–231. doi: 10.1126/science.265.5169.228
- Stuiver, M., Pearson, G. W., and Braziunas, T. (1986). Radiocarbon age calibration of marine samples back to 9000 Cal yr BP. *Radiocarbon* 28 (2B), 980–1021. doi: 10.1017/s0033822200060264
- Stuiver, M., Reimer, P. J., and Braziunas, T. F. (1998). High-precision radiocarbon age calibration for terrestrial and marine samples. *Radiocarbon* 40 (3), 1127–1151. doi: 10.1017/s0033822200019172
- Tamura, T., Saito, Y., Nguyen, V. L., Ta, T. K. O., Bateman, M. D., Matsumoto, D., et al. (2012). Origin and evolution of inter-distributary delta plains; insights from Mekong river delta. *Geology* 40 (4), 303–306. doi: 10.1130/g32717.1
- Tamura, T., Saito, Y., Sieng, S., Ben, B., Kong, M., Sim, I., et al. (2009). Initiation of the Mekong river delta at 8 ka: evidence from the sedimentary succession in the Cambodian lowland. *Quatern. Sci. Rev.* 28 (3–4), 327–344. doi: 10.1016/j.quascirev.2008.10.010
- Tanabe, S., Saito, Y., Lan Vu, Q., Hanebuth, T. J. J., Lan Ngo, Q., and Kitamura, A. (2006). Holocene evolution of the song Hong (Red river) delta system, northern Vietnam. *Sediment. Geol.* 187 (1–2), 29–61. doi: 10.1016/j.sedgeo.2005.12.004
- Wang, Z. H., Jones, B. G., Chen, T., Zhao, B. C., and Zhan, Q. (2013). A raised OIS 3 sea level recorded in coastal sediments, southern changjiang delta plain, China. *Quatern. Res.* 79 (3), 424–438. doi: 10.1016/j.yqres.2013.03.002
- Wang, Z. H., Saito, Y., Zhan, Q., Nian, X. M., Pan, D. D., Wang, L., et al. (2018). Three-dimensional evolution of the Yangtze river mouth, China during the Holocene: impacts of sea level, climate and human activity. *Earth-Sci. Rev.* 185, 938–955. doi: 10.1016/j.earscirev.2018.08.012
- Wang, Z. B., Yang, S. Y., Tang, H. Y., Zheng, Y. L., Wang, H. Y., Zhang, Z. X., et al. (2022). Revisit the sedimentary stratigraphic evolution and environmental changes on the outer shelf of the East China Sea since MIS 5. *Front. Mar. Sci.* 9. doi: 10.3389/fmars.2022.863245
- Wang, F., Zhang, W. G., Nian, X. M., Ge, C., Zhao, X. Q., Cheng, Q. Z., et al. (2019). Refining the late-Holocene coastline and delta development of the northern Yangtze river delta: Combining historical archives and OSL dating. *Holocene* 29 (9), 1439–1449. doi: 10.1177/0959683619854522
- Wei, X., Mo, W. Y., and Wu, C. Y. (2011). Analysis on the sedimentation rates and depositional environment of the pearl river delta area since Holocene. *Acta Sedimentol. Sin.* 29 (2), 328–335. doi: 10.14027/j.cnki.cjxb.2011.02.017
- Wei, X., and Wu, C. Y. (2011). Holocene Delta evolution and sequence stratigraphy of the pearl river delta in south China. *Sci. China Earth Sci.* 54 (10), 1523–1541. doi: 10.1007/s11430-011-4238-6
- Wei, X., and Wu, C. Y. (2014). Long-term process-based morphodynamic modeling of the pearl river delta. *Ocean. Dynamics* 64 (12), 1753–1765. doi: 10.1007/s10236-014-0785-7
- Woodroffe, C. D., Nicholls, R. J., Saito, Y., Chen, Z., and Goodbred, S. L. (2006). “Landscape variability and the response of Asian megadeltas to environmental change,” in *Global change and integrated coastal management* (Berlin: Springer), 277–314. doi: 10.1007/1-4020-3628-0_10
- Woodroffe, C. D. (2000). Deltaic and estuarine environments and their late quaternary dynamics on the sunda and sahur shelves. *J. Asian Earth Sci.* 18 (4), 393–413. doi: 10.1016/s1367-9120(99)00074-7
- Wu, C. Y., Ren, J., Bao, Y., Lei, Y. P., and Shi, H. Y. (2007). “A long-term morphological modeling study on the evolution of the pearl river delta, network system, and estuarine bays since 6000 yr B.P.,” in *Coastline changes: Interrelation of*

- climate and geological processes* (Colorado: Geological Society of America), 426, 199–210.
- Wu, Z. Y., Saito, Y., Zhao, D. N., Zhou, J. Q., Cao, Z. Y., Li, S. J., et al. (2016). Impact of human activities on subaqueous topographic change in lingding bay of the pearl river estuary, China, during 1955–2013. *Sci. Rep.* 6, 37742. doi: 10.1038/srep37742
- Wu, C. Y., and Wei, X. (2021). From drowned valley to delta: Discrimination and analysis on issues of the formation and evolution of the zhujiang river delta (in Chinese with English abstract). *Acta Oceanol. Sin.* 43 (1), 1–26. doi: 10.12284/hyxb2021019
- Wu, C. Y., Xing, W., Jie, R., Yun, B., Zhigang, H., Yiaping, L., et al. (2010). Morphodynamics of the rock-bound outlets of the pearl river estuary, south China — a preliminary study. *J. Mar. Syst.* 82, S17–S27. doi: 10.1016/j.jmarsys.2010.02.002
- Wu, M. S., Zong, Y. Q., Mok, K. M., Cheung, K. M., Xiong, H. X., and Huang, G. Q. (2017). Holocene Hydrological and sea surface temperature changes in the northern coast of the south China Sea. *J. Asian Earth Sci.* 135, 268–280. doi: 10.1016/j.jseas.2017.01.004
- Xiong, H. X., Zong, Y. Q., Huang, G. Q., and Fu, S. Q. (2018a). Sedimentary responses to Holocene sea-level change in a shallow marine environment of southern China. *J. Asian Earth Sci.* 166, 95–106. doi: 10.1016/j.jseas.2018.07.033
- Xiong, H. X., Zong, Y. Q., Huang, G. Q., and Fu, S. Q. (2020). Human drivers accelerated the advance of pearl river deltaic shoreline in the past 7500 years. *Quatern. Sci. Rev.* 246. doi: 10.1016/j.quascirev.2020.106545
- Xiong, H. X., Zong, Y. Q., Qian, P., Huang, G. Q., and Fu, S. Q. (2018b). Holocene Sea-level history of the northern coast of south China Sea. *Quatern. Sci. Rev.* 194, 12–26. doi: 10.1016/j.quascirev.2018.06.022
- Xu, Y. T., Lai, Z. P., and Li, C. A. (2019). Sea-Level change as the driver for lake formation in the Yangtze plain – a review. *Global Planet Change* 181. doi: 10.1016/j.gloplacha.2019.102980
- Xu, X. L., Li, H. W., Tang, L. J., Lai, Z. P., Xu, G. J., Zhang, X. H., et al. (2020). Chronology of a Holocene core from the pearl river delta in southern China. *Front. Earth Sci.* 8. doi: 10.3389/feart.2020.00262
- Xu, X. L., Zhong, J. M., Huang, X. M., Li, H. W., Ding, Z. J., and Lai, Z. P. (2022). Age comparison by luminescence using quartz and feldspar on core HPQK01 from the pearl river delta in China. *Quatern. Geochronol.* 71. doi: 10.1016/j.quageo.2022.101320
- Yao, Y., Zhan, W., Liu, Z., Zhang, Z., Zhan, M., and Sun, J. (2013). Neotectonics and its relations to the evolution of the pearl river delta, guangdong, China. *J. Coast. Res.* 66, 1–11. doi: 10.2112/si_66_1
- Yi, L., Lai, Z. P., Yu, H. J., Xu, X. Y., Su, Q., Yao, J., et al. (2012). Chronologies of sedimentary changes in the south bohai Sea, China: constraints from luminescence and radiocarbon dating. *Boreas* 42 (2), 267–284. doi: 10.1111/j.1502-3885.2012.00271.x
- Yim, W. W. S., Hilgers, A., Huang, G. Q., and Radtke, U. (2008). Stratigraphy and optically stimulated luminescence dating of subaerially exposed quaternary deposits from two shallow bays in Hong Kong, China. *Quatern. Int.* 183 (1), 23–39. doi: 10.1016/j.quaint.2007.07.004
- Yim, W. W. S., Huang, G. Q., Fontugne, M. R., Hale, R. E., Paterne, M., Pirazzoli, P. A., et al. (2006). Postglacial sea-level changes in the northern south China Sea continental shelf: Evidence for a post-8200 calendar yr BP meltwater pulse. *Quatern. Int.* 145–146, 55–67. doi: 10.1016/j.quaint.2005.07.005
- Yim, W. W. S., Ivanovich, M., and Yu, K. F. (1990). Young age bias of radiocarbon dates in pre-holocene marine deposits of Hong Kong and implications for pleistocene stratigraphy. *Geo-Mar. Lett.* 10 (3), 165–172. doi: 10.1007/bf02085932
- Yi, L., Ye, X. Y., Chen, J. B., Li, Y., Long, H., Wang, X. L., et al. (2014). Magnetostratigraphy and luminescence dating on a sedimentary sequence from northern East China Sea: Constraints on evolutionary history of eastern marginal seas of China since the early pleistocene. *Quatern. Int.* 349, 316–326. doi: 10.1016/j.quaint.2014.07.038
- Yu, Z. X. (2017). *The age of the lower transgression cycle in the pearl river delta and its implication of Sea-level changes and neotectonic movements*. Ph. D. thesis Sun Yat-sen University Guangzhou.
- Yu, Z. X., Zhang, K., Liang, H., and Li, Z. Y. (2016). Late quaternary tectonic movements in the pearl river delta, china, revealed from stratigraphic profiles (in Chinese with English abstract). *Trop. Geogr.* 36, 334–342. doi: 10.13284/j.cnki.rddl.002850
- Yu, F. L., Zong, Y. Q., Lloyd, J. M., Huang, G. Q., Leng, M. J., Kendrick, C., et al. (2010). Bulk organic $\delta^{13}C$ and C/N as indicators for sediment sources in the pearl river delta and estuary, southern China. *Estua. Coast. Shelf. Sci.* 87 (4), 618–630. doi: 10.1016/j.ecss.2010.02.018
- Zaitlin, B. A., Dalrymple, R. W., and Boyd, R. (1994). “The stratigraphic organization of incised-valley systems associated with relative Sea-level change,” in *Incised-valley systems: Origin and sedimentary sequences*. Eds. R. W. Dalrymple, B. A. Zaitlin and A. Peter. (Virginia: Society for Sedimentary Geology), 51, 45–60. doi: 10.2110/pec.94.12.0045
- Zhang, W., Xu, Y., Hoitink, A. J. F., Sassi, M. G., Zheng, J. H., Chen, X. W., et al. (2015). Morphological change in the pearl river delta, China. *Mar. Geol.* 363, 202–219. doi: 10.1016/j.margeo.2015.02.012
- Zhao, X., Chen, S., Huang, C., Zeng, M., Chen, W., Dong, H., et al. (2014). Facies architecture and depositional model of a macrotidal incised valley succession (Qiantang River estuary, eastern China), and differences from other macrotidal systems (in Chinese with English abstract). *Geol. Bulletin China* 33 (10) 1635–1641. doi: 10.3969/j.issn.1671-2552.2014.10.023
- Zheng, Z., Ma, T., Roberts, P., Li, Z., Yue, Y., Peng, H., et al. (2021). Anthropogenic impacts on late Holocene land-cover change and floristic biodiversity loss in tropical southeastern Asia. *Proc. Natl. Acad. Sci. U.S.A.* 118 (40). doi: 10.1073/pnas.2022210118
- Zong, Y. Q., Huang, G. Q., Switzer, A. D., Yu, F. L., and Yim, W. W. S. (2009a). An evolutionary model for the Holocene formation of the pearl river delta, China. *Holocene* 19 (1), 129–142. doi: 10.1177/09596836080898957
- Zong, Y. Q., Huang, K. Y., Yu, F. L., Zheng, Z., Switzer, A., Huang, G. Q., et al. (2012). The role of sea-level rise, monsoonal discharge and the palaeo-landscape in the early Holocene evolution of the pearl river delta, southern China. *Quatern. Sci. Rev.* 54, 77–88. doi: 10.1016/j.quascirev.2012.01.002
- Zong, Y. Q., Lloyd, J. M., Leng, M. J., Yim, W. W. S., and Huang, G. Q. (2006). Reconstruction of Holocene monsoon history from the pearl river estuary, southern China, using diatoms and carbon isotope ratios. *Holocene* 16 (2), 251–263. doi: 10.1191/0959683606hl911rp
- Zong, Y. Q., Yim, W. W. S., Yu, F. L., and Huang, G. Q. (2009b). Late quaternary environmental changes in the pearl river mouth region, China. *Quatern. Int.* 206 (1–2), 35–45. doi: 10.1016/j.quaint.2008.10.012
- Zong, Y. Q., Yu, F. L., Huang, G. Q., Lloyd, J. M., and Yim, W. W. S. (2010). Sedimentary evidence of late Holocene human activity in the pearl river delta, China. *Earth Surface Processes Landforms* 35 (9), 1095–1102. doi: 10.1002/esp.1970
- Zong, Y., Huang, G., Li, X. Y., and Sun, Y. Y. (2015). Late Quaternary tectonics, sea-level change and lithostratigraphy along the northern coast of the South China Sea. *Geol. Soc. Lond. Spec. Publ.* 429(1), 123–136. doi: 10.1144/sp429.1
- Zong, Y. Q., Zheng, Z., Huang, K. Y., Sun, Y. Y., Wang, N., Tang, M., et al. (2013). Changes in sea level, water salinity and wetland habitat linked to the late agricultural development in the pearl river delta plain of China. *Quatern. Sci. Rev.* 70, 145–157. doi: 10.1016/j.quascirev.2013.03.020